Geophysical Journal International

Geophys. J. Int. (2016) **205,** 427–439
GJI Seismology

doi: 10.1093/gji/ggw024

Highly accurate stability-preserving optimization of the Zener viscoelastic model, with application to wave propagation in the presence of strong attenuation

Émilie Blanc,[1,2] Dimitri Komatitsch,[1] Emmanuel Chaljub,[3] Bruno Lombard[1] and Zhinan Xie[1,4]

[1] *LMA, CNRS UPR* 7051, *Aix-Marseille University, Centrale Marseille, F*-13453 *Marseille cedex* 13, *France. E-mail: komatitsch@lma.cnrs-mrs.fr*
[2] *Division of Scientific Computing, Department of Information Technology, Uppsala University, Box* 337, *SE*-751 05 *Uppsala, Sweden*
[3] *Université Grenoble Alpes and CNRS, ISTerre, BP* 53, *F*-38041 *Grenoble, France*
[4] *Institute of Engineering Mechanics, China Earthquake Administration, Harbin* 150080, *China*

Accepted 2016 January 15. Received 2015 December 20; in original form 2015 November 14

SUMMARY

This paper concerns the numerical modelling of time-domain mechanical waves in viscoelastic media based on a generalized Zener model. To do so, classically in the literature relaxation mechanisms are introduced, resulting in a set of the so-called memory variables and thus in large computational arrays that need to be stored. A challenge is thus to accurately mimic a given attenuation law using a minimal set of relaxation mechanisms. For this purpose, we replace the classical linear approach of Emmerich & Korn with a nonlinear optimization approach with constraints of positivity. We show that this technique is more accurate than the linear approach. Moreover, it ensures that physically meaningful relaxation times that always honour the constraint of decay of total energy with time are obtained. As a result, these relaxation times can always be used in a stable way in a modelling algorithm, even in the case of very strong attenuation for which the classical linear approach may provide some negative and thus unusable coefficients.

Key words: Numerical solutions; Numerical approximations and analysis; Body waves; Seismic attenuation; Computational seismology; Wave propagation.

1 INTRODUCTION

Taking dissipation mechanisms, that is, viscoacoustic or viscoelastic behaviour into account is often important in fields that involve acoustic or elastic wave propagation. This has led to significant research effort for instance in seismology, seismic wave propagation and imaging in the oil and gas industry, non-destructive industrial evaluation based on ultrasonic waves, or medical imaging. A large number of articles can be found in the literature about modelling of viscoelastic media characterized by their quality factor Q, with recent reviews available for instance in Petersson & Sjögreen (2012) and Carcione (2014). Of particular interest is the case of a Q factor that is constant over a wide range of frequencies because that is observed in many cases of practical interest (see e.g. Liu *et al.* 1976; Dahlen & Tromp 1998; Komatitsch & Tromp 1999).

In pioneering work, Liu *et al.* (1976) demonstrated that a finite and constant quality factor can be modelled by superimposing N standard linear solid (SLS) damping mechanisms. Day & Minster (1984) developed a Padé approximant of the viscoelastic modulus for time-domain wave propagation simulations. Emmerich & Korn (1987) then showed that the rheological model of a generalized Maxwell body can be used to represent the rational approximation of the viscoelastic modulus and developed a linear least-squares technique to compute the coefficients of the rational approximation involved (i.e. the points and weights that are needed in the case of time-domain simulations) in an optimized fashion. This latter work has resulted in an improved approximation of a viscoelastic solid having a given quality factor Q and has become the classical way of representing such a material. It has been used in numerous subsequent articles, for example, Carcione *et al.* (1988a,b), Kristek & Moczo (2003), Komatitsch *et al.* (2004), Moczo & Kristek (2005), Käser *et al.* (2007), Martin & Komatitsch (2009), Savage *et al.* (2010), Lombard & Piraux (2011), Dhemaied *et al.* (2011) and Petersson & Sjögreen (2012). It is also worth mentioning that Moczo & Kristek (2005) proved the equivalence between the different rheological models mentioned previously, as also analysed by Cao & Yin (2014). Because of this equivalence, in what follows for simplicity we will call it the Zener model and will mostly refer to the formulation of Carcione (2014) for that model.

In the context of time-domain simulations, these methods are often expensive in terms of memory storage when implemented numerically because they require the use of the so-called

memory variables that need to be stored and marched in time (see e.g. Moczo & Kristek 2005; Carcione 2014). To alleviate this, Day (1998), Day & Bradley (2001), Graves & Day (2003) and van Driel & Nissen-Meyer (2014) have suggested spreading the relaxation mechanisms and thus the related memory variables over adjacent grid points, using a single mechanism per grid point and trying to get a good approximation of the damping behaviour in average over a local volume, in particular when attenuation is weak (van Driel & Nissen-Meyer 2014). However, there are open questions regarding the overall accuracy of such an approach, in particular when propagating waves over a large number of wavelengths, which is very often the case in practice. Kristek & Moczo (2003) have also pointed out the fact that the presence of discontinuities, that is, of interfaces in the material model under study, can lead to inaccuracies in this spreading technique.

In practice, the Zener model requires fitting $Q(\omega)$ over a range of angular frequencies $[\omega_{\min}, \omega_{\max}]$, which implies determining a set of N points and N weights. As mentioned above, this is classically done based on the linear approach of Emmerich & Korn (1987), in which one sets the N points and then optimizes and solves for the N weights. Casula & Carcione (1992) have proposed an approximation to simplify the way of computing the weights, in particular in the case of low-loss solids. However, two important drawbacks can appear with this technique. First, the accuracy of the approach can be relatively poor, that is, the error compared with the real constant Q can be large when the frequency range under study is large and/or when the number of relaxation mechanisms N used is small. This amounts to introducing a physical modelling error, independent of the numerical error induced in addition by the chosen numerical scheme. Second, some weights can be negative because the linear approach of Emmerich & Korn (1987) does not enforce their positivity. This is particularly true when attenuation is strong (say $Q < 20$ or so), which is a case that can occur for instance in site effect and earthquake hazard assessment studies (poorly consolidated sediments), in soil-structure interaction studies where values of the critical damping ratio $\xi = \frac{1}{2Q}$ larger than 5 per cent are often considered in the structures, as well as in non-destructive industrial testing or medical imaging. In such a case the physical and also mathematical constraint of decay of total energy with time can be broken, as we will see in Section 2, and using such negative weights can make wave propagation modelling algorithms become unstable. Peyrusse *et al.* (2014) pointed out the problem of negative weights in the approach of Emmerich & Korn (1987) and proposed to impose their positivity in the inversion, as also addressed by Withers *et al.* (2015). However, they did not invert jointly for the points and weights and found that their approach was at best as accurate as that of Emmerich & Korn (1987).

Alternative approaches exist to represent viscoelastic damping mechanisms and to compute their coefficients. For instance, Xu & McMechan (1998) used simulated annealing to find the weights of the Zener body, the relaxation times being evenly distributed in logarithmic scale over N points in the band of angular frequencies. Russo & Zollo (2003) developed an analytical approach for optimization of the relaxation times; however, they used a less general relaxation function by assigning the same ratio of relaxed and unrelaxed moduli to all Zener bodies, and they did not introduce the positivity of the weights as a constraint. Liu & Archuleta (2006) used a simulated annealing approach to compute the relaxation points and weights for only two extreme values of the quality factor, $Q = 5$ and $Q = 5000$, and proposed a regression methodology to derive the coefficients for intermediate values of Q. However, they also did not impose the positivity of the weights as a constraint and their approximation of the Q values is limited to a 5 per cent accuracy. Furthermore, their expression of the viscoelastic modulus is different from the classical one of, for example, Moczo & Kristek (2005), Lombard & Piraux (2011), Petersson & Sjögreen (2012) and Carcione (2014). Bielak *et al.* (2011) introduced an internal friction model with optimized memory efficiency based on a Kelvin–Voigt body put in parallel with two Maxwell bodies and managed to mimic an almost constant Q quality factor over two decades in frequency. Other attempts at improving the coefficient optimization process can be found in the literature: Robertsson *et al.* (1994) and Robertsson (1996) developed a quasi-analytical approach, but an important limitation is that it is valid only when Q is large; Asvadurov *et al.* (2004) minimized the error in L_∞ norm in an elegant way, but their approach is quite involved and, more importantly, valid for a constant Q only.

In this paper, our goal is thus to develop a nonlinear optimization technique that (i) will be significantly more accurate than the classical approach of Emmerich & Korn (1987) and (ii) will always lead to physically meaningful relaxation times that honour the constraint of decay of total energy with time, by enforcing the positivity of all the coefficients obtained, including in the case of strong attenuation, thus ensuring stable simulations. Compared to Emmerich & Korn (1987) we will not set the points but rather solve and optimize for them jointly with the weights, imposing strict positivity as a constraint in the process. Instead of solving for N unknowns, we will thus solve for $2N$ unknowns. Having more degrees of freedom to solve for, we will be able to significantly improve the accuracy of the approximation. This strategy has successfully been used in other fields such as viscoelastic models in solid mechanics (Rekik & Brenner 2011) and high-frequency poroelasticity (Blanc *et al.* 2013). To some extent, this idea has some similarities with switching from Newton–Cotes (trapezoidal, Simpson...) quadrature to Gauss quadrature in numerical integration in order to get a more accurate integration rule by determining optimized points and weights instead of weights only. The methodology that we will introduce is independent of the numerical scheme used to solve the wave equation in time, that is, it is general and can be used in numerical techniques as diverse as finite differences, finite elements, spectral elements, discontinuous Galerkin, etc. The coefficients are computed once and for all in a preprocessing step.

The paper is organized as follows: in Section 2.1, we briefly recall some elementary notions about viscoelasticity and discuss the decay of total energy with time. In Section 2.2, we recall the approach of Emmerich & Korn (1987) and reformulate it within our framework. In Section 2.3, we introduce the nonlinear optimization approach that will allow us to define the new methodology. In Section 3, we perform numerical experiments to show the dispersion and quality factor curves obtained, which illustrates the improved accuracy of the results. Finally, in Section 4, we perform a numerical experiment for 3-D wave propagation in a tabular medium, which confirms the robustness and the improved accuracy of the nonlinear optimization approach.

2 PHYSICAL MODELLING

As mentioned above, viscoelastic models are widely used in the case of the propagation of acoustic or seismic waves in dissipative media, among other applications. The 2-D or 3-D linear viscoelastic wave equation then writes:

$$\rho \frac{\partial^2 \mathbf{u}}{\partial t^2} = \nabla \cdot \boldsymbol{\sigma} + \mathbf{f}, \tag{1}$$

where $\boldsymbol{\rho}$ is the distribution of density and $\mathbf{u}$ denotes the displacement field produced by the source $\mathbf{f}$. The symmetric stress tensor $\boldsymbol{\sigma}$ is linearly related to the strain tensor $\boldsymbol{\varepsilon} = \frac{1}{2}(\boldsymbol{\nabla}\mathbf{u} + (\boldsymbol{\nabla}\mathbf{u})^T)$ by Hooke's law, which in an elastic, anisotropic linear solid may be written in the form

$$\boldsymbol{\sigma} = \mathbf{c} : \boldsymbol{\varepsilon}\,, \tag{2}$$

where the colon denotes a double tensor contraction operation. The elastic properties of the medium are determined by the fourth-order elastic tensor $\mathbf{c}$, which in an isotropic medium is $c_{ijk\ell} = \lambda\delta_{ij}\delta_{k\ell} + \mu(\delta_{ik}\delta_{j\ell} + \delta_{i\ell}\tilde{}\delta_{jk})$, where δ is the Kronecker delta symbol and λ and μ are the two Lamé parameters, related to the pressure and shear wave celerities and to density by $\mu = \rho\, c_s^2$ and $\lambda = \rho\, c_p^2 - 2\mu$. In an attenuating medium, Hooke's law (2) needs to be modified such that the stress is determined by the entire strain history:

$$\boldsymbol{\sigma}(t) = \int_{-\infty}^{t} \frac{\partial}{\partial t}\mathbf{c}(t - t') : \boldsymbol{\varepsilon}(t')\, \mathrm{d}t'\,. \tag{3}$$

In the 1-D case without attenuation this reduces to

$$\begin{aligned} \rho\, \frac{\partial^2 u}{\partial t^2} &= \frac{\partial \sigma}{\partial x} + f \\ \varepsilon &= \frac{\partial u}{\partial x} \\ \sigma &= (\lambda + 2\,\mu)\varepsilon \end{aligned} \tag{4}$$

with scalar unknowns, and in an attenuating medium Hooke's law becomes

$$\sigma(t) = \int_{-\infty}^{t} \frac{\partial}{\partial t}(\lambda(t - t') + 2\,\mu(t - t'))\,\varepsilon(t')\, \mathrm{d}t'\,. \tag{5}$$

2.1 Constitutive law

Let us briefly recall elementary notions about viscoelasticity in 1-D. In higher spatial dimensions, the discussion below is then straightforwardly applied to the compressional and shear relaxation functions, respectively. The reader is referred, for example, to Carcione (2014) for a detailed presentation. The integro-differential expression of 1-D linear viscoelasticity writes

$$\sigma = \psi * \frac{\partial \varepsilon}{\partial t}, \tag{6}$$

where $*$ denotes time convolution. The relaxation function of the Zener model writes

$$\psi(t) = E_r \left(1 - \frac{1}{N} \sum_{\ell=1}^{N} \left(1 - \frac{\tau_{\varepsilon\ell}}{\tau_{\sigma\ell}} \right) \mathrm{e}^{-\frac{t}{\tau_{\sigma_\ell}}} \right) H(t), \tag{7}$$

where E_r is the relaxed modulus, N is the number of relaxation mechanisms, $\tau_{\varepsilon\ell}$ and $\tau_{\sigma\ell}$ are relaxation times and H is the Heaviside step function. It is worth mentioning that the $1/N$ factor in eq. (7) is not present in earlier publications (Liu *et al.* 1976; Carcione *et al.* 1988a,b). This has been changed in Carcione (2001) and Moczo & Kristek (2005) as well as in many subsequent publications. The model with the $1/N$ factor is physically more meaningful because the model without it cannot be represented by mechanical elements, since it requires a spring with negative constant (Casula & Carcione 1992); but calculations not shown here demonstrate that these two ways of expressing the Zener model are equivalent. Another issue that is sometimes found in the literature is that waves speed up instead of slowing down when attenuation is turned on because the reference used is the relaxed state instead of the more traditional unrelaxed state (e.g. in Carcione 1993).

At $t = 0$, the relaxation function (7) is equal to the unrelaxed modulus E_u

$$E_u = \frac{1}{N} \sum_{\ell=1}^{N} \frac{\tau_{\varepsilon\ell}}{\tau_{\sigma\ell}}\, E_r. \tag{8}$$

As time increases, ψ decreases monotonically from E_u to E_r, and as frequency increases, the phase velocity increases monotonically from c_0 to c_∞ defined by

$$c_0 = \sqrt{\frac{E_r}{\rho}}, \qquad c_\infty = \sqrt{\frac{E_u}{\rho}}. \tag{9}$$

Instead of writing the constitutive law as a convolution product (6), one can equivalently use the differential form

$$\begin{cases} \sigma = \displaystyle\sum_{\ell=1}^{N} \sigma_\ell, \\ \sigma_\ell + \tau_{\sigma\ell}\, \dfrac{\partial \sigma \ell}{\partial t} = E_{r\ell} \left(\varepsilon + \tau_{\varepsilon\ell}\, \dfrac{\partial \varepsilon}{\partial t} \right), \qquad \ell = 1, \ldots, N, \\ E_{r\ell} = \dfrac{E_r}{N}\,. \end{cases} \tag{10}$$

This form is useful to prove the decay of energy (Bécache *et al.* 2004).

Property 1. Let us define

$$\mathcal{E} = \mathcal{E}_1 + \mathcal{E}_2 + \mathcal{E}_3, \tag{11}$$

with

$$\begin{aligned} \mathcal{E}_1 &= \frac{1}{2} \int_{\mathbb{R}} \rho\, v^2\, \mathrm{d}x, \\ \mathcal{E}_2 &= \frac{1}{2} \int_{\mathbb{R}} E_r \left(\frac{\partial u}{\partial x} \right)^2 \mathrm{d}x, \\ \mathcal{E}_3 &= \frac{1}{2} \sum_{\ell=1}^{N} \int_{\mathbb{R}} \frac{\tau_{\sigma\ell}}{E_{r\ell}\,(\tau_{\varepsilon\ell} - \tau_{\sigma\ell})} \left(\sigma_\ell - E_{r\ell} \frac{\partial u}{\partial x} \right)^2 \mathrm{d}x, \end{aligned} \tag{12}$$

where $v = \frac{\partial u}{\partial t}$ is velocity and ρ is density. $\mathcal{E}_1$ corresponds to the kinetic energy, $\mathcal{E}_2$ to the elastic potential energy in the relaxed state and $\mathcal{E}_3$ to the sum of the inelastic potential energies. The total energy $\mathcal{E}$ then obeys

$$\frac{\mathrm{d}\mathcal{E}}{\mathrm{d}t} = -\sum_{\ell=1}^{N} \int_{\mathbb{R}} \frac{1}{E_{r\ell}\,(\tau_{\varepsilon\ell} - \tau_{\sigma\ell})} \left(\sigma_\ell - E_{r\ell} \frac{\partial u}{\partial x} \right)^2 \mathrm{d}x. \tag{13}$$

To prove (13), the conservation of momentum in eq. (4) combined with system (10) can be written as

$$\rho\, \frac{\partial v}{\partial t} = \frac{\partial \sigma}{\partial x}, \tag{14a}$$

$$\sigma = \sum_{\ell=1}^{N} \sigma_\ell, \tag{14b}$$

$$\sigma_\ell + \tau_{\sigma\ell}\, \frac{\partial \sigma \ell}{\partial t} = E_{r\ell} \left(\frac{\partial u}{\partial x} + \tau_{\varepsilon\ell}\, \frac{\partial v}{\partial x} \right), \qquad \ell = 1, \ldots, N. \tag{14c}$$

There is a typo in the original paper in Equations (24) and (26): missing i omega factor, fixed here.

Let us multiply eq. (14a) by v and integrate by parts:

$$\int_{\mathbb{R}} \rho\, v\, \frac{\partial v}{\partial t}\, \mathrm{d}x + \int_{\mathbb{R}} \frac{\partial v}{\partial x}\, \sigma\, \mathrm{d}x = 0. \tag{15}$$

We can then transform the stress σ into σ_ℓ thanks to eq. (14b)

$$\int_{\mathbb{R}} \rho\, v\, \frac{\partial v}{\partial t}\, \mathrm{d}x + \sum_{\ell=1}^{N} \int_{\mathbb{R}} \frac{\partial v}{\partial x}\, \sigma_\ell\, \mathrm{d}x = 0, \tag{16}$$

and split the resulting equation into two terms:

$$\int_{\mathbb{R}} \underbrace{\left(\rho\, v\, \frac{\partial v}{\partial t} + E_r\, \frac{\partial u}{\partial x}\, \frac{\partial}{\partial t}\left(\frac{\partial u}{\partial x}\right)\right)}_{\Delta_1} \mathrm{d}x$$

$$+ \sum_{\ell=1}^{N} \int_{\mathbb{R}} \underbrace{\left(\sigma_\ell - E_{r\ell}\, \frac{\partial u}{\partial x}\right) \frac{\partial v}{\partial x}}_{\Delta_2}\, \mathrm{d}x = 0. \tag{17}$$

Eq. (14c) then yields

$$\sigma_\ell - E_{r\ell}\, \frac{\partial u}{\partial x} + \tau_{\sigma\ell}\, \frac{\partial}{\partial t}\left(\sigma_\ell - E_{r\ell}\, \frac{\partial u}{\partial x}\right) = E_{r\ell}\, (\tau_{\varepsilon\ell} - \tau_{\sigma\ell})\, \frac{\partial v}{\partial x}, \tag{18}$$

and thus

$$\frac{\partial v}{\partial x} = \frac{1}{E_{r\ell}\, (\tau_{\varepsilon\ell} - \tau_{\sigma\ell})} \left(\sigma_\ell - E_{r\ell}\, \frac{\partial u}{\partial x} + \tau_{\sigma\ell}\, \frac{\partial}{\partial t}\left(\sigma_\ell - E_{r\ell}\, \frac{\partial u}{\partial x}\right)\right). \tag{19}$$

Injecting eq. (19) into Δ_2 in eq. (17) and using straightforward algebra recovers eq. (13).

An important remark follows from Property 1: if $\tau_{\varepsilon\ell} > \tau_{\sigma\ell} > 0$ $\forall \ell$ then $\mathcal{E}$ in eq. (11) is a definite-positive quadratic form, and

$$\frac{\mathrm{d}\mathcal{E}}{\mathrm{d}t} < 0\,. \tag{20}$$

The condition $\tau_{\varepsilon\ell} > \tau_{\sigma\ell} > 0$ $\forall \ell$ is therefore a sufficient condition to obtain a decreasing total energy. It is worth mentioning that we have not shown that it is necessary in the mathematical sense because we cannot exclude that there can be cases in which the sum in eq. (13) remains positive even if some of the coefficients are negative. In higher spatial dimensions a similar energy analysis can be performed; computations are slightly more involved but the conclusion is unchanged (Bécache *et al.* 2004). Let us also mention that a standard linear solid in which $\tau_\sigma > \tau_\varepsilon$ instead of $\tau_\varepsilon > \tau_\sigma$ is sometimes called an anti-Zener body (Mainardi 2010). Such a body is non-causal, that is, its energy in the unrelaxed state is smaller than its energy in the relaxed state; This means that one of its two springs has a negative modulus.

2.2 Linear optimization

The relaxation function of the generalized Zener model involves $2N + 1$ parameters. The relaxed modulus E_r can be deduced from the phase velocity at zero frequency (eq. 9). Determination of the relaxation times $\tau_{\varepsilon\ell}$ and $\tau_{\sigma\ell}$ is more involved. The most classical approach originates in the work of Emmerich & Korn (1987), which we are going to briefly recall. For the sake of simplicity, we perform the calculations with new unknowns:

$$\kappa_\ell = \frac{1}{N}\left(\frac{\tau_{\varepsilon\ell}}{\tau_{\sigma\ell}} - 1\right), \qquad \theta_\ell = \frac{1}{\tau_{\sigma\ell}}, \tag{21}$$

from which the original coefficients can be recovered using

$$\tau_{\varepsilon\ell} = \frac{1 + N\,\kappa_\ell}{\theta_\ell}, \qquad \tau_{\sigma\ell} = \frac{1}{\theta_\ell}. \tag{22}$$

These coefficients will also be useful in future sections because imposing $\tau_{\varepsilon\ell} > \tau_{\sigma\ell} > 0$ $\forall \ell$ simply means imposing $\kappa_\ell > 0$ and $\theta_\ell > 0$. The viscoelasticity modulus $M = \mathcal{F}(\frac{\partial \Psi}{\partial t})$, where $\mathcal{F}$ is the Fourier transform in time, is deduced from (7):

$$M(\omega) = E_r \left(1 + i\,\omega \sum_{\ell=1}^{N} \frac{\kappa_\ell}{\theta_\ell + i\,\omega}\right). \tag{23}$$

We determine the relaxed modulus E_r so that the phase velocity of the Zener model equals c_r at a given reference frequency f_r: $c(\omega_r) \equiv c_r$, with $\omega_r = 2\,\pi\, f_r$. The wavenumber is

$$k = \left(\frac{\rho\,\omega^2}{M(\omega)}\right)^{1/2} = \sqrt{\frac{\rho}{E_r}}\,\omega \left(1 + \sum_{\ell=1}^{N} \frac{i\,\omega\kappa_\ell}{\theta_\ell + i\omega}\right)^{-1/2}. \tag{24}$$

Denoting $\Re(k)$ the real part of k, the phase velocity is

$$c(\omega) = \frac{\omega}{\Re(k)} = \sqrt{\frac{E_r}{\rho}}\, \mathcal{F}(\omega), \tag{25}$$

with

$$\mathcal{F}(\omega) = 1/\Re\left\{\left(1 + \sum_{\ell=1}^{N} \frac{i\,\omega\kappa_\ell}{\theta_\ell + i\omega}\right)^{-1/2}\right\}. \tag{26}$$

The requirement $c(\omega_r) \equiv c_r$ is then reached by taking

$$E_r = \frac{\rho\, c_r^2}{\mathcal{F}(\omega_r)}. \tag{27}$$

The quality factor Q is defined as the ratio of the imaginary part to the real part of M. Its reciprocal writes

$$Q^{-1}(\omega) = \frac{\displaystyle\sum_{\ell=1}^{N} \frac{\omega\,\theta_\ell\,\kappa_\ell}{\theta_\ell^2 + \omega^2}}{1 + \displaystyle\sum_{\ell=1}^{N} \frac{\omega^2\,\kappa_\ell}{\theta_\ell^2 + \omega^2}}. \tag{28}$$

The main idea in Emmerich & Korn (1987) is then to minimize the distance between $Q^{-1}(\omega)$ and a given $Q_{\mathrm{ref}}^{-1}(\omega)$ in a band of angular frequencies $[\omega_{\min}, \omega_{\max}]$, which of course depends on the spectrum of the source under study, that is, on the frequency content of the data or experiment that one wants to model. For this purpose in Emmerich & Korn (1987) the relaxation frequencies θ_ℓ are evenly distributed over N points in logarithmic scale

$$\theta_\ell = \omega_{\min} \left(\frac{\omega_{\max}}{\omega_{\min}}\right)^{\frac{\ell-1}{N-1}}, \qquad \ell = 1, \ldots, N, \tag{29}$$

in the band of angular frequencies $[\omega_{\min}, \omega_{\max}]$. The coefficients κ_ℓ are then obtained by identifying the reciprocal of the quality factor (28) with a given $Q_{\mathrm{ref}}^{-1}(\omega)$. From eq. (28), one obtains the set of equations

$$\sum_{\ell=1}^{N} \frac{\omega_k \left(\theta_\ell - \omega_k\, Q_{\mathrm{ref}}^{-1}(\omega_k)\right)}{\theta_\ell^2 + \omega_k^2}\, \kappa_\ell = Q_{\mathrm{ref}}^{-1}(\omega_k), \quad k = 1, \ldots, K, \tag{30}$$

where the angular frequencies are distributed linearly on a logarithmic scale of K points

$$\omega_k = \omega_{\min} \left(\frac{\omega_{\max}}{\omega_{\min}}\right)^{\frac{k-1}{K-1}}, \quad k = 1, \ldots, K. \tag{31}$$

If $K = N$, one obtains a square linear system. The choice $K = 2N - 1$ is often made (Groby & Tsogka 2006), leading to an overdetermined system. Nothing in this method prevents from obtaining negative values $\kappa_\ell < 0$ when solving eq. (30), yielding $\tau_{\varepsilon\ell} < \tau_{\sigma\ell}$ via eq. (22), which is unsuitable both physically and mathematically as mentioned in Property 1. In practice, this can (and does) happen in particular when N is large, typically $N \geq 5$ or so, as we will see in Section 3.

Emmerich & Korn (1987) suggest that ω_k/ω_{k-1} should be chosen equal to about 10 in practice, however, such a choice is not always convenient or even possible in all situations because it means that when the number of mechanisms N is large then the total bandwidth should be extremely large (10^{N-1}), while in some situations in order to improve accuracy one wants to have standard linear solids that are located much closer to one another and be able to increase N to improve the accuracy of the approximation without having to use a large distance $\omega_k/\omega_{k-1} \simeq 10$ between two mechanisms. Also, from a mathematical point of view imposing that ω_k/ω_{k-1} be around 10 does not automatically ensure the positivity of the coefficients obtained; if positivity is not imposed explicitly as a constraint, there is no particular mathematical reason for it to be ensured in practice.

2.3 Optimization with constraints

Let us introduce the objective function

$$\mathcal{J}\left(\{\kappa_\ell, \theta_\ell\}\,;\, N,\, K\right) = \sum_{k=1}^{K} \left(\sum_{\ell=1}^{N} \frac{\omega_k\, Q_{\mathrm{ref}}(\omega_k)\left(\theta_\ell - \omega_k\, Q_{\mathrm{ref}}^{-1}(\omega_k)\right)}{\theta_\ell^2 + \omega_k^2}\, \kappa_\ell - 1 \right)^2 . \tag{32}$$

Minimizing eq. (32) with respect to the κ_ℓ only recovers the Emmerich & Korn (1987) expressions (30). Here we propose to minimize eq. (32) in terms of both variables, imposing decay of total energy with time as in eq. (20), that is, imposing $\tau_{\varepsilon\ell} > \tau_{\sigma\ell} > 0\ \forall \ell$, which in turn means imposing the positivity constraints $\kappa_\ell > 0$ and $\theta_\ell > 0$. We introduce the additional constraint $\theta_\ell < \theta_{\max}$ in order to avoid too large values of θ_ℓ, which could result in stiff equations and thus in numerical instabilities in the time-marching of memory variables (Blanc *et al.* 2013).

These $3N$ constraints are relaxed by setting $\kappa_\ell = \kappa_\ell'^2$ and $\theta_\ell = \theta_\ell'^2$ and solving the following problem with only N constraints:

$$\min_{\{\kappa_\ell', \theta_\ell'\}} \mathcal{J}\left(\{\kappa_\ell'^2, \theta_\ell'^2\}\,;\, N,\, K\right), \quad \text{with } \theta_\ell'^2 \leq \theta_{\max} \text{ for } \ell = 1, \ldots, N. \tag{33}$$

As problem (33) is nonlinear and non-quadratic with respect to abscissas θ_ℓ', to solve it we resort to the *SolvOpt* algorithm (Kappel & Kuntsevich 2000; Rekik & Brenner 2011), which is based on the iterative Shor's method (Shor 1985). As starting values for that iterative optimization technique we use the values $\kappa_\ell'^{(0)}$ and $\theta_\ell'^{(0)}$ obtained based on the Emmerich & Korn (1987) procedure (29)–(30) (even if some of them are negative, since our nonlinear optimization procedure will then ensure positivity).

To determine the $2N$ coefficients κ_ℓ' and θ_ℓ', the minimal number of relaxation frequencies is $K = 2N$. In practice, we have observed better accuracy when taking the larger value $K = 4N$. The angular frequencies ω_k are chosen evenly spaced in logarithmic scale over the optimization band $[\omega_{\min}, \omega_{\max}]$, as in the linear approach, and thus eq. (31) remains valid.

3 NUMERICAL VALIDATION OF THE APPROACH

3.1 Approximation and coefficients obtained

Let us illustrate the improved accuracy of the approximation obtained as well as the fact that the coefficients κ_ℓ and θ_ℓ obtained are always positive. To do so, let us perform several numerical experiments with different numbers of relaxation mechanisms N. Optimization is performed over $K = 4N$ angular frequencies ω_k (31), as explained in Section 2.3. We set the lower and upper bounds of the angular frequency range to

$$\omega_{\min} = \omega_c/10, \qquad \omega_{\max} = 10\,\omega_c, \tag{34}$$

where $\omega_c = 2\pi f_c$ is the dominant angular frequency of the source.

We first take a constant quality factor $Q_{\mathrm{ref}} = 5$ and a dominant frequency of the source $f_c = 1.5$ Hz. Fig. 1 shows the exact value of Q_{ref}^{-1} and the numerical approximation (28) obtained using optimization based on $N = 2$ to $N = 7$ relaxation mechanisms in the angular frequency band $[\omega_{\min}, \omega_{\max}]$. In the interval of optimization, the linear approach of Emmerich & Korn (1987) yields oscillations whereas the nonlinear optimization with constraints gives a curve that is almost constant and fits the exact value very well.

The numerical values of the coefficients κ_ℓ and θ_ℓ obtained with $N = 6$ are given in Table 1. The κ_5 weight is negative in the linear Emmerich & Korn (1987) procedure, which could lead to unstable results if used in a numerical simulation, as illustrated in Section 4, because the set of coefficients does not necessarily honour the constraint of decay of energy with time of eq. (20).

To evaluate the effect of the optimization more quantitatively, it is useful to introduce the following quantities:

(1) u_{ex}^{Q} the unknown exact solution of the model with a truly constant Q_{ref} factor, which obeys a fractional-order partial differential equation (Carcione *et al.* 2002);

(2) u_{ex}^{Z} the unknown exact solution of the Zener model approximation of that constant Q_{ref}, which obeys a standard partial differential equation with memory variables;

(3) u_{num}^{Z} the known numerical solution of the partial differential equation with memory variables, obtained using the numerical scheme selected to solve the wave eq. (1).

The triangular inequality then yields the total error

$$\varepsilon_t = ||u_{\mathrm{ex}}^{Q} - u_{\mathrm{num}}^{Z}|| \leq \underbrace{||u_{\mathrm{ex}}^{Q} - u_{\mathrm{ex}}^{Z}||}_{\varepsilon_m} + \underbrace{||u_{\mathrm{ex}}^{Z} - u_{\mathrm{num}}^{Z}||}_{\varepsilon_n}, \tag{35}$$

in which ε_n is the numerical error due to discretization. That error depends on the numerical scheme chosen to discretize the wave

Table 1. Coefficients of eq. (21) obtained when resorting to (a) the method of Emmerich & Korn (1987) and (b) nonlinear optimization with constraints, for a quality factor $Q = 5$ modelled with $N = 6$ relaxation mechanisms. One can note that one gets a negative weight for $\ell = 5$ in the case of the linear approach of Emmerich & Korn (1987).

(a)	κ_ℓ	θ_ℓ	(b)	κ_ℓ	θ_ℓ
$\ell = 1$	$+2.81\,10^{-1}$	$1.50\,10^{-1}$	$\ell = 1$	$+2.93\,10^{-1}$	$9.18\,10^{-2}$
$\ell = 2$	$+1.29\,10^{-1}$	$3.77\,10^{-1}$	$\ell = 2$	$+1.92\,10^{-1}$	$3.57\,10^{-1}$
$\ell = 3$	$+1.07\,10^{-1}$	$9.46\,10^{-1}$	$\ell = 3$	$+2.00\,10^{-1}$	$1.01\,10^{0}$
$\ell = 4$	$+3.54\,10^{-1}$	$2.38\,10^{0}$	$\ell = 4$	$+2.26\,10^{-1}$	$2.75\,10^{0}$
$\ell = 5$	$-1.00\,10^{-1}$	$5.97\,10^{0}$	$\ell = 5$	$+2.84\,10^{-1}$	$7.75\,10^{0}$
$\ell = 6$	$+7.85\,10^{-1}$	$1.50\,10^{1}$	$\ell = 6$	$+7.39\,10^{-1}$	$3.38\,10^{1}$

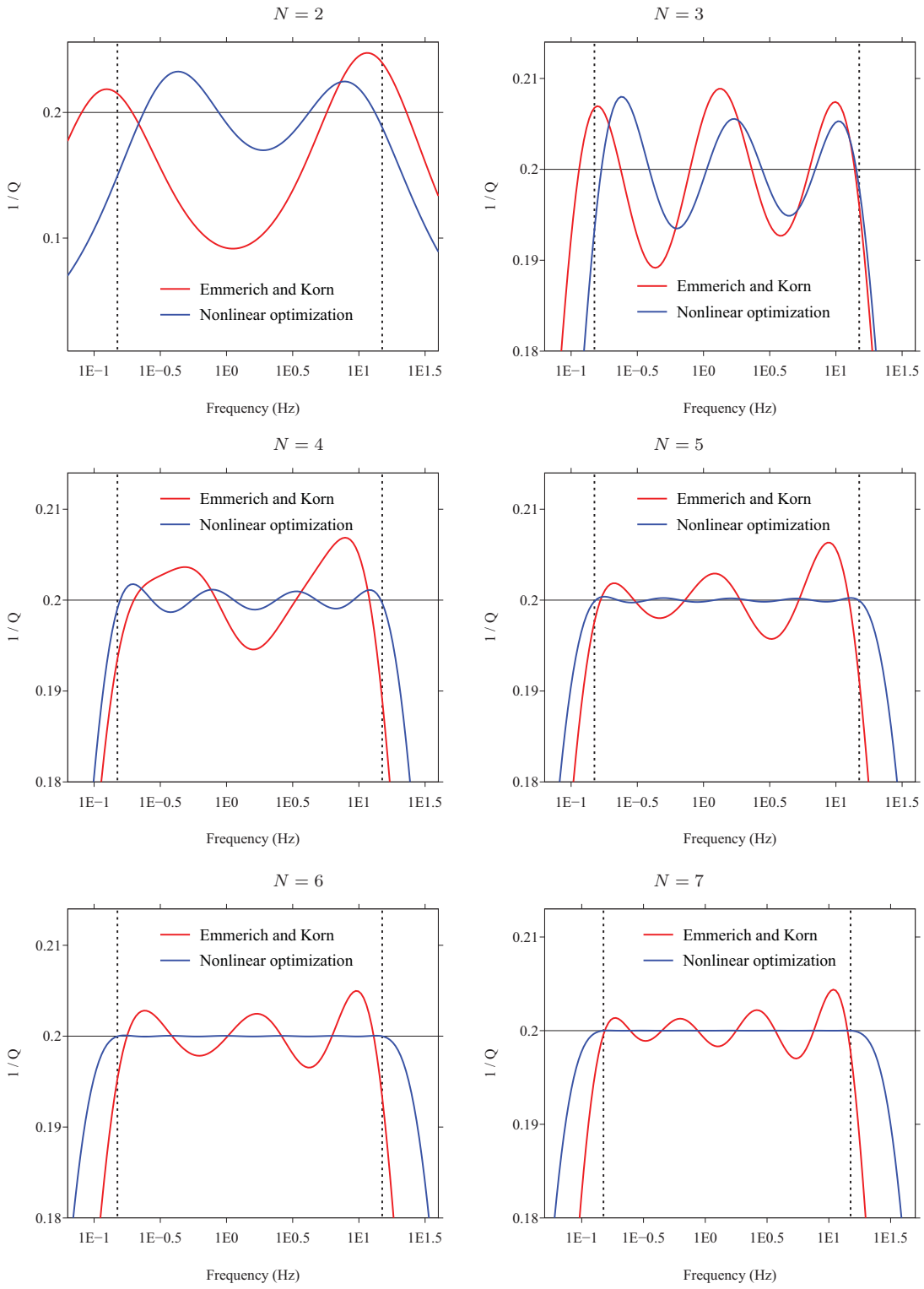

Figure 1. Reciprocal of the quality factor when using a Zener approximation with $N = 2$ (upper left) to $N = 7$ (bottom right) relaxation mechanisms based on the linear approach of Emmerich & Korn (1987) (red line) and nonlinear optimization (blue line). The vertical dotted lines denote the interval of optimization $[f_{\min}, f_{\max}]$. The horizontal axis is in logarithmic scale.

equation and can be analysed using standard numerical analysis tools (which is classical in the literature and out of the scope of this paper). Here we focus on the physical modelling error ε_m, which is related to the quality of the optimization process:

$$\varepsilon_m \sim ||Q_{\text{ref}}^{-1}(\omega) - Q^{-1}(\omega)||_2 \tag{36}$$

in the interval of optimization. Values of ε_m for $Q_{\text{ref}} = 5$ and various values of the number of relaxation mechanisms N are given in Table 2. With $N = 6$ we get $\varepsilon_m = 1.21$ per cent in the case of Emmerich & Korn (1987) and $\varepsilon_m = 0.0156$ per cent in the case of nonlinear optimization with constraints. When making the number of relaxation mechanisms N vary from 2 to 6 we get the relative

Table 2. Relative physical modelling error (36) in the case of the linear approach of Emmerich & Korn (1987) and in the case of nonlinear optimization, when making the number of relaxation mechanisms vary from $N = 2$ to $N = 7$. Nonlinear optimization always leads to more accurate results.

N	Linear optimization	Nonlinear optimization
2	$\varepsilon_m = 34.2$ per cent	$\varepsilon_m = 10.7$ per cent
3	$\varepsilon_m = 3.08$ per cent	$\varepsilon_m = 2.17$ per cent
4	$\varepsilon_m = 1.99$ per cent	$\varepsilon_m = 0.42$ per cent
5	$\varepsilon_m = 1.49$ per cent	$\varepsilon_m = 0.08$ per cent
6	$\varepsilon_m = 1.21$ per cent	$\varepsilon_m = 0.0156$ per cent
7	$\varepsilon_m = 0.86$ per cent	$\varepsilon_m = 0.0030$ per cent

errors of Table 2. For $N = 2$ we get improvement, for $N = 3$ the difference is less pronounced but then for $N \geq 4$ the difference becomes significant again. These errors are displayed in Fig. 2. When nonlinear optimization is used the error keeps decaying in a very significant fashion, while in the case of the linear approach of Emmerich & Korn (1987) it does not.

Let us illustrate the effect of the physical modelling error ε_m on time-domain results of 1-D wave propagation. The only linear and causal model of viscoelasticity having a constant quality factor Q was introduced by Kjartansson (1979). We compare the exact solution for the velocity obtained with that truly constant Q model (u_{ex}^{Q}), which is the reference solution, with the exact solution obtained with the Zener model approximation of that constant Q (u_{ex}^{Z}). These exact solutions are computed semi-analytically based on Fourier synthesis. Details about how to compute the solution in the case of the Zener model can be found in appendix D of Favrie *et al.* (2015). We consider a homogeneous 1-D domain extending from $x_{\min} = -5000$ m to $x_{\max} = +5000$ m. The constant density is $\rho = 2000$ kg m^{-3}, the reference frequency is $f_r = 1.5$ Hz and the celerity at that frequency is $c_r = 2000$ m s^{-1}. The source is a Ricker wavelet force with dominant frequency $f_c = f_r$ located at $x = 0$. Fig. 3 shows the time history of velocity recorded at two receivers r_1 and r_2 located in $x_{r1} = 1000$ m and $x_{r2} = 3000$ m, respectively. Since dispersion is a cumulative effect, as expected the errors are more pronounced after a larger distance of propagation. In the case of linear optimization a visible error remains even when using $N = 4$ relaxation mechanisms; on the contrary an almost perfect agreement is obtained if nonlinear optimization is used with $N = 4$ relaxation mechanisms.

3.2 Dispersion curves

The dispersion of the Kjartansson (1979) model is

$$c(\omega) = c_r \left(\frac{\omega}{\omega_r} \right)^{\frac{1}{\pi} \arctan \frac{1}{Q}} . \tag{37}$$

An important remark from eq. (37) is that one can see that the phase velocity of this model is not bounded at infinite frequency, contrary to that of the Zener model. A consequence is that in such a model the reference velocity needs to be given at a finite frequency, it cannot be an unrelaxed value at infinite frequency as in the Zener model.

Fig. 4 compares the phase velocities of the Zener model (obtained with the two methods of optimization) with the reference phase velocity of the Kjartansson (1979) model. The parameters used are $c_r = 2000$ m s^{-1}, $f_r = 1.5$ Hz and $Q = 5$. The optimization is performed in the frequency range $[f_c/10, 10f_c]$, where $f_c = f_r$. The choice $f_r = f_c$ is natural, it amounts to choosing the dominant frequency of the source as the reference frequency. For $N = 2$ relaxation mechanisms, the linear optimization largely overestimates the phase velocity of the Zener model (a), whereas nonlinear optimization underestimates the phase velocity of the Zener model at $f > f_c$ (b). For $N = 4$, a good agreement is observed between the Zener model and the Kjartansson (1979) model if nonlinear optimization is used (b).

3.3 Case of a non-constant Q factor

We now select a varying quality factor (e.g. Dahlen & Tromp 1998)

$$Q(\omega) = Q_0 \left(\frac{\omega}{\omega_0} \right)^{-\alpha} , \tag{38}$$

with $Q_0 = 20$, $f_0 = 1.5$ Hz, $\omega_0 = 2\pi f_0$ and $\alpha = 0.1$. Since the exponent is negative, this leads to $1/Q$ increasing with frequency, that is, to higher attenuation at higher frequency. As in Fig. 1 for the case of a constant Q, in Fig. 5 we show the exact value of $Q^{-1}(\omega)$ and the numerical approximation (28) obtained using optimization

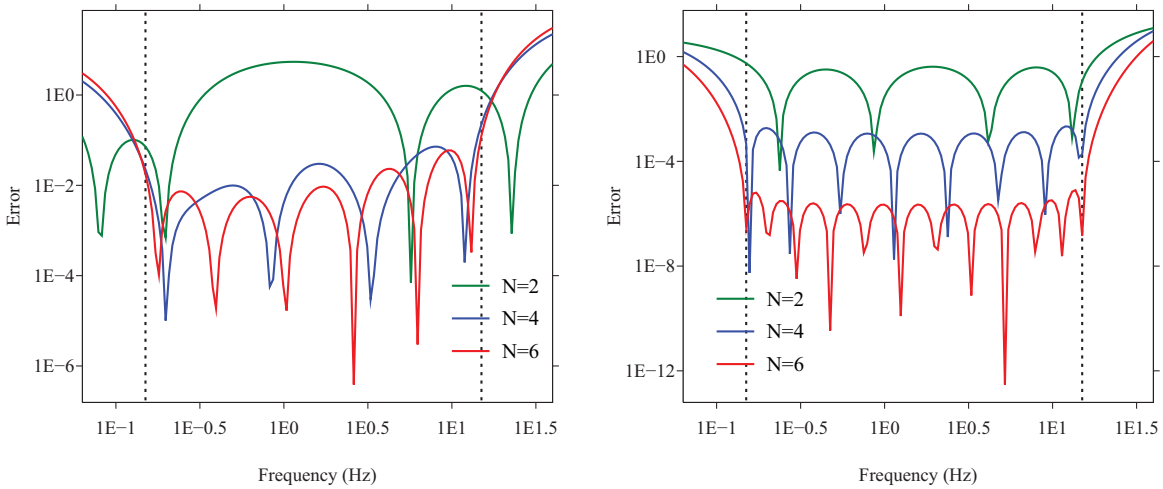

Figure 2. Value of the objective function of eq. (32) as a function of frequency, using a Zener approximation with $N = 2$ (green curve), $N = 4$ (blue curve) and $N = 6$ (red curve) relaxation mechanisms, with the linear approach of Emmerich & Korn (1987) (left) and with nonlinear optimization (right). The vertical dotted lines denote the interval of optimization $[f_{\min}, f_{\max}]$. Both axes are in logarithmic scale. Note that the vertical logarithmic scale has about twice more decades on the right figure than on the left figure, that is, the error levels are very significantly different.

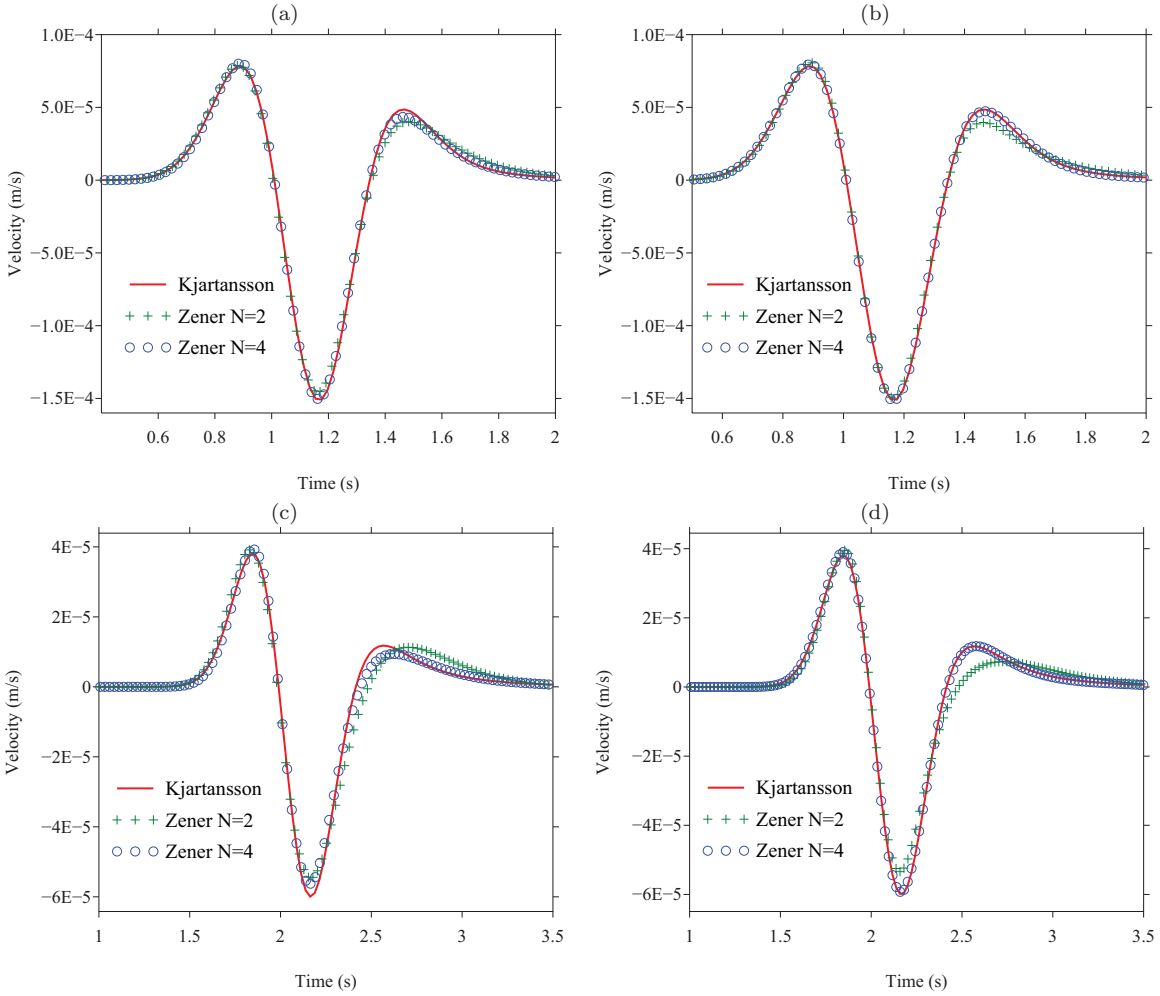

Figure 3. Time history of velocity recorded at receivers r_1 (top) and r_2 (bottom), comparing the exact solution of the Kjartansson (1979) model (red curve) to the exact solution of the Zener model obtained with linear optimization (left row) and with nonlinear optimization (right row), for $N = 2$ (green curve) and $N = 4$ (blue curve) relaxation mechanisms.

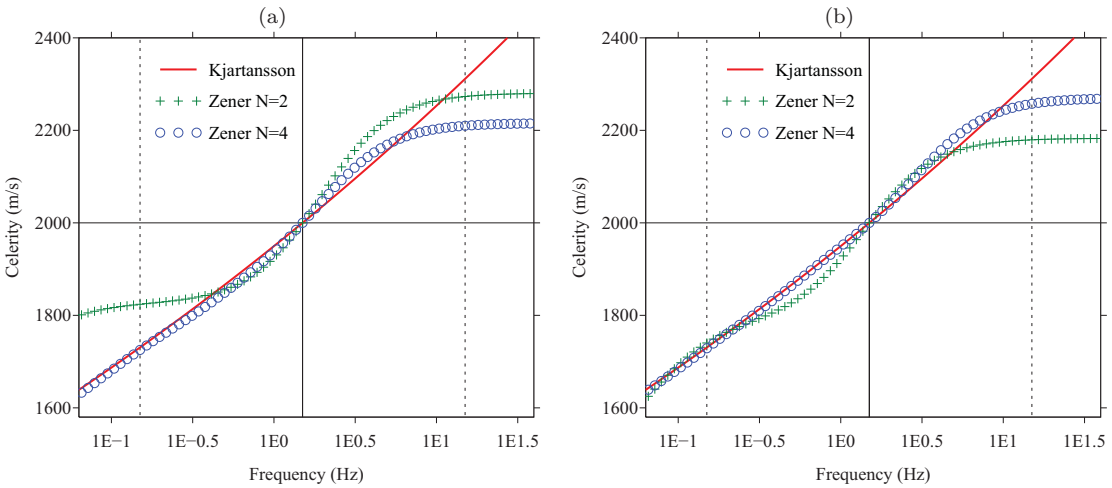

Figure 4. Dispersion curves obtained with linear optimization (a) and with nonlinear optimization (b) in the case of the Kjartansson (1979) model (red curve), the Zener model with $N = 2$ relaxation mechanisms (green curve) and the Zener model with $N = 4$ relaxation mechanisms (blue curve). The solid vertical line indicates the reference frequency $f_r = 1.5$ Hz. The vertical dotted lines denote the frequency range $[f_c/10, 10f_c]$ in which optimization is performed. The horizontal line denotes the celerity $c(f_r) = 2000$ m s^{-1} on which all the models are locked, that is, where they are by definition identical.

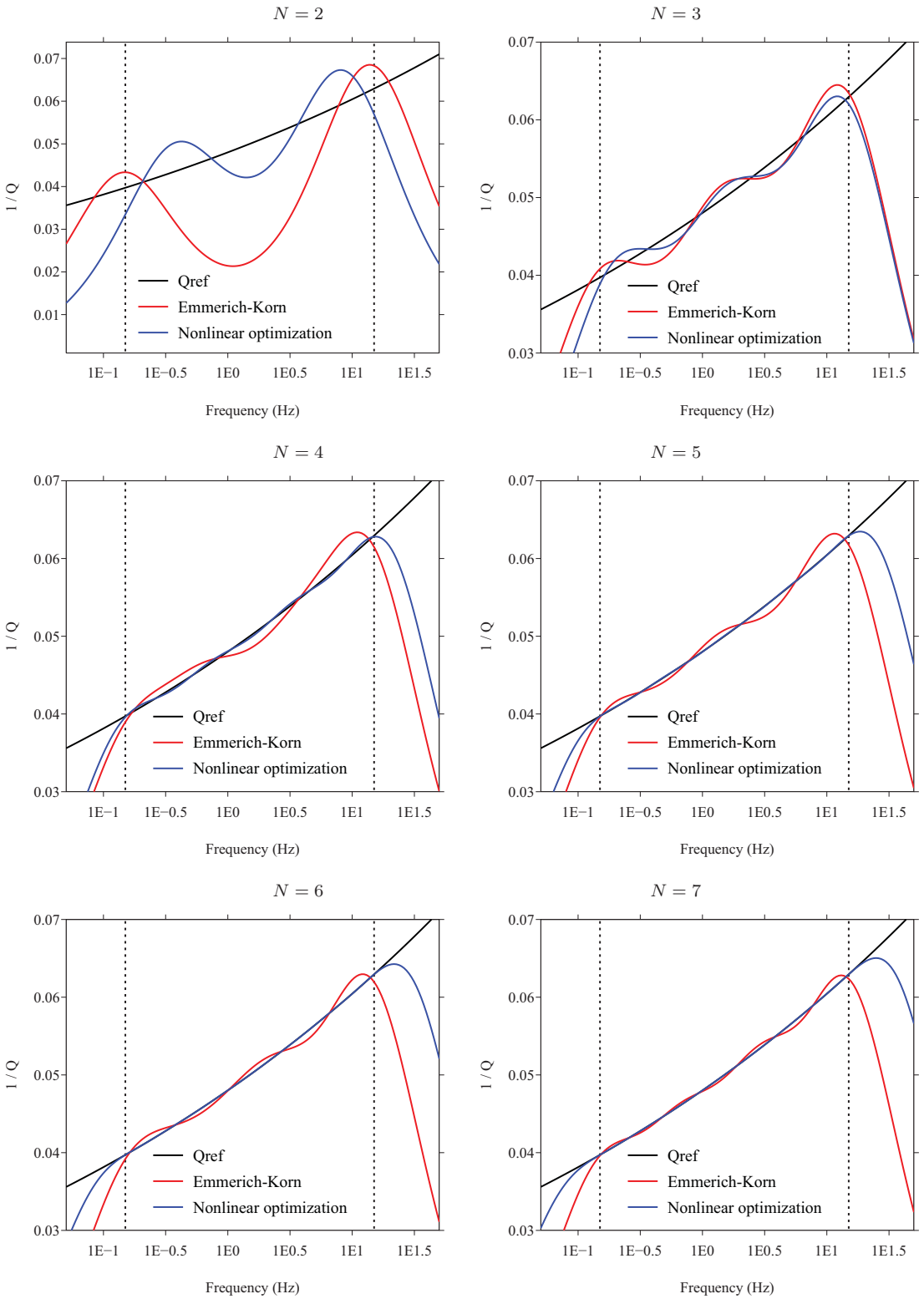

Figure 5. Same as Fig. 1 but for a non-constant quality factor $Q(\omega) = Q_0(\frac{\omega}{\omega_0})^{-\alpha}$, with $Q_0 = 20, f_0 = 1.5$ Hz, $\omega_0 = 2\pi f_0$ and $\alpha = 0.1$.

based on $N = 2$ to $N = 7$ relaxation mechanisms in the angular frequency band $[\omega_{\min}, \omega_{\max}]$. In the interval of optimization, the linear approach of Emmerich & Korn (1987) yields more oscillations than the result obtained with the nonlinear optimization approach with constraints.

4 VALIDATION FOR 3-D WAVE PROPAGATION IN A LAYER-CAKE MEDIUM

In Section 3, we have illustrated how the choice of the relaxation times in the Zener model affects the accuracy of time domain

Table 3. Layered viscoelastic model used in the validation examples of Section 4. The L_i, $i = 1 \ldots 3$ refer to the sedimentary layers and B to the surrounding bedrock. h stands for layer thickness, V_S, V_P, Q_S, Q_P stand for S and P seismic velocities and quality factors and ρ stands for mass density.

	h (m)	V_P (m s^{-1})	V_S (m s^{-1})	ρ (kg m^{-3})	Q_P	Q_S
L_1	17.3	1500	200	2100	40	20
L_2	72.5	1800	350	2100	70	35
L_3	115.6	2500	650	2200	130	65
B	–	4500	2600	2600	∞	∞

solutions of the viscoelastic wave equation in a homogeneous medium. Let us now turn to a more realistic example of 3-D propagation in a tabular medium with strong contrasts in viscoelastic properties. For this purpose, we consider the viscoelastic medium described in Table 3. The elastic version of this model was used by Chaljub *et al.* (2015) to study the accuracy of numerical predictions of earthquake ground motion in the Mygdonian basin in northern Greece. The model consists in a stiff elastic half-space overlaid by three sedimentary layers with lower seismic impedances, which cause large amplification of earthquake ground motion (the so-called site effects). The shear quality factors in the sediments are approximated by a simple, frequency-independent scaling from the shear velocities, $Q_S = V_S/10$, as done in site effect studies in the (general) situation in which no other constraints on intrinsic attenuation can be used; the P quality factors are defined by $Q_P = 2\,Q_S$.

The viscoelastic medium is excited by a double-couple point source with a vertical strike-slip focal mechanism. The source is set at 80 m depth in order to excite high-frequency surface waves propagating within the sedimentary layers. In realistic cases, those surface waves would be generated locally by conversion of incoming body waves at strong lateral heterogeneities located close to the surface (for example at basin edges) and would contribute to the amplification and duration lengthening of ground motion. The source time function is a step with a rising time $\tau = 0.1$ s. It radiates a far-field displacement with a flat spectrum up to 1 Hz and gradual decay between 1 Hz and 10 Hz.

The computations are performed with the AXITRA software package (Coutant 1989), which implements a discrete wavenumber method (Bouchon 1981). As in Section 3, we compute the solutions for the truly constant Q model of Kjartansson (1979), and for Zener models with different numbers of mechanisms, whose relaxation times are obtained based either on linear or nonlinear optimization. We use a reference frequency $f_r = 1$ Hz and solve for the relaxation times of the Zener models in the two-decade frequency range $[f_r/10, 10f_r]$.

Fig. 6(a) shows 25 s of horizontal ground acceleration computed at 4-km epicentral distance for the truly constant Q model (black line) and for the Zener models with $N = 3$ mechanisms and relaxation times inverted using linear (red line) or nonlinear (blue line) optimization. Note that the overall agreement between traces is quite good even for late surface waves, mainly because anchoring the dispersion of the different models at the reference frequency has the effect of minimizing phase misfit. The differences in amplitude can be analysed by comparing Fourier amplitude spectra (Fig. 6b). The solutions of the Zener models either underpredict (around $f_r = 1$ Hz) or overpredict (around 2.5 Hz) the amplitude of the constant Q solution, as expected from Fig. 1. The maximum differences reach about 10 per cent around the dominant, reference frequency. A more precise measure is to quantify time–frequency misfits, or goodness-of-fit scores as proposed by Kristeková *et al.* (2009). When applied to very similar signals, the envelope (resp. phase) misfits or goodness-of-fit scores mainly reflect the differences or similarities in amplitude (resp. phase) between the traces. In Fig. 6c, we plot the envelope goodness-of-fit scores as a function of time. Each goodness-of-fit value $g(t)$ corresponds to a frequency average over the range [0.2–5 Hz] of the envelope time–frequency misfit, $m(t)$,

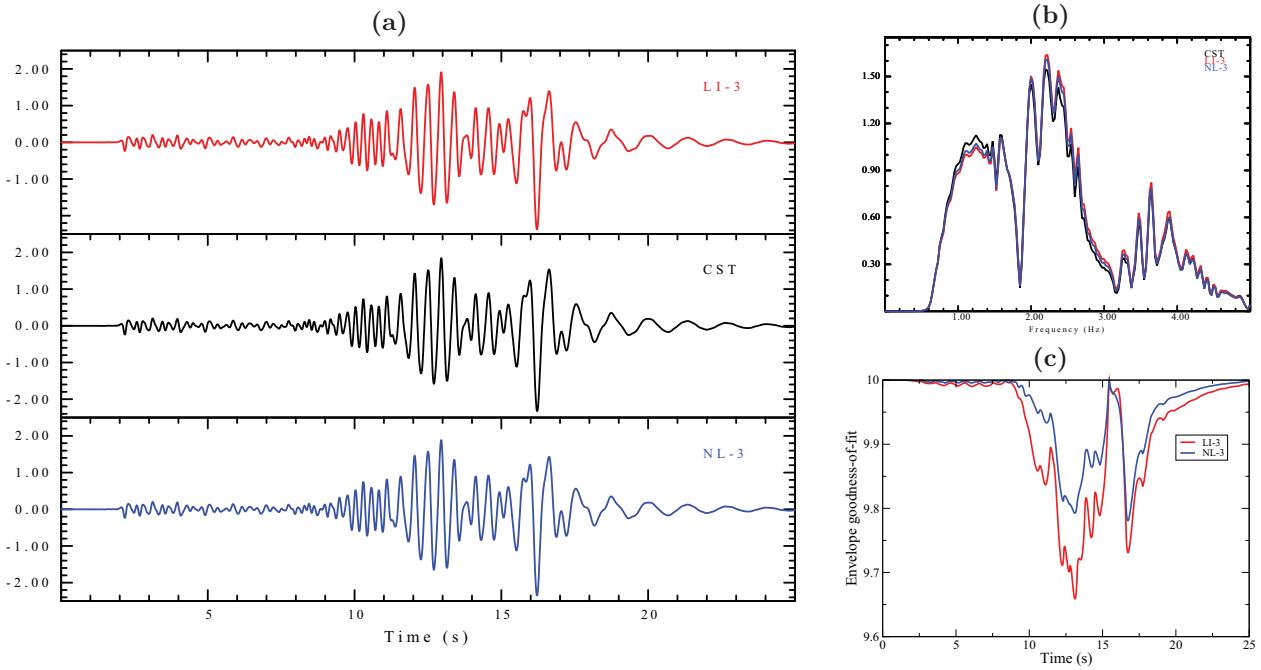

Figure 6. (a) Time evolution of horizontal ground acceleration in cm s^{-2} at 4-km epicentral distance for a constant Q model (black line) and for the Zener model with $N = 3$ relaxation mechanisms obtained based on linear (red) or nonlinear (blue) optimization. (b) Corresponding Fourier amplitude spectra. (c) Time evolution of the envelope goodness-of-fit with respect to the reference solution of the constant Q model.

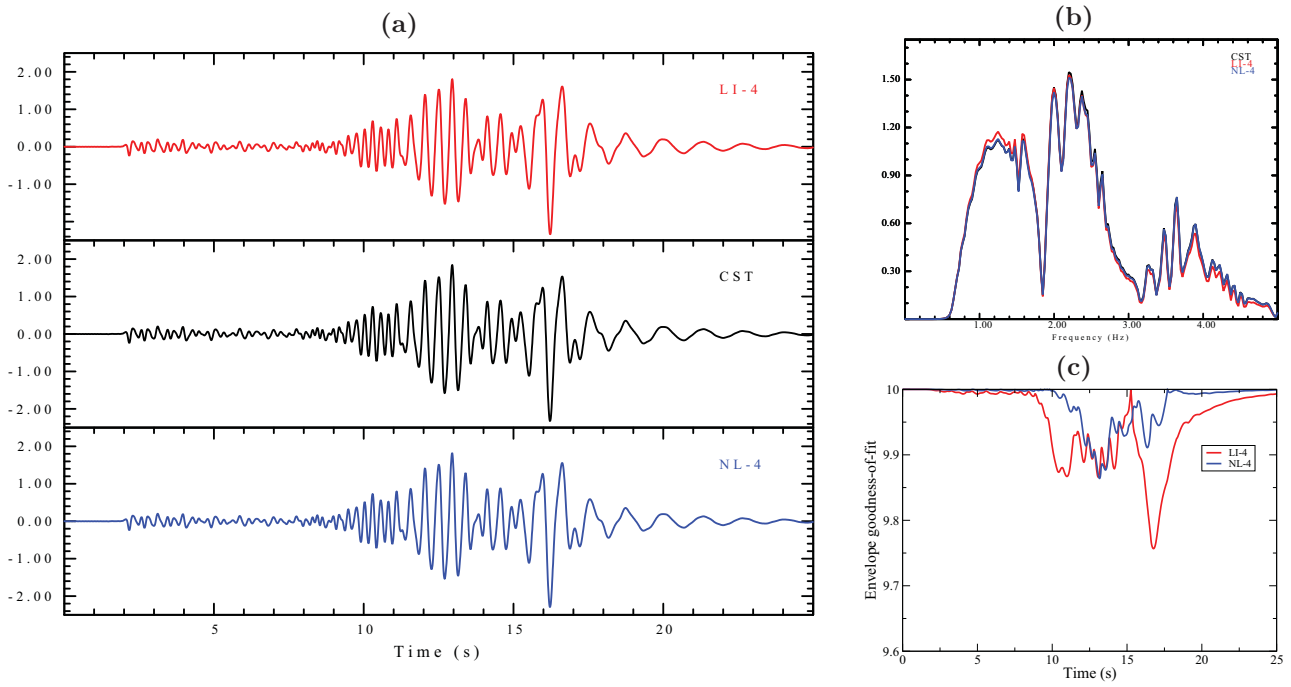

Figure 7. Same as Fig. 6 but using $N = 4$ relaxation mechanisms.

Table 4. Average envelope (E) and phase (P) goodness-of-fits of horizontal ground acceleration for the Zener viscoelastic models with relaxation times obtained based on linear and nonlinear optimization.

N	Linear optimization	Nonlinear optimization
3	$E = 9.36$ $P = 9.76$	$E = 9.57$ $P = 9.82$
4	$E = 9.64$ $P = 9.88$	$E = 9.84$ $P = 9.93$
6	$E = 9.83$ $P = 9.90$	$E = 9.90$ $P = 9.95$
10	$E = 9.89$ $P = 9.94$	$E = 9.90$ $P = 9.96$

which is further scaled to a score between 0 (no fit) and 10 (perfect fit) based on the nonlinear mapping $g(t) = 10 \exp[-m(t)]$. The figure shows that nonlinear optimization of the relaxation times in the Zener model always yields a more accurate approximation of the constant Q model, even for $N = 3$.

From the analysis of Fig. 1, we expect that this trend should be even more pronounced if we increase the number of relaxation mechanisms. This is indeed the case for the results obtained with $N = 4$ relaxation mechanisms, which are shown in Fig. 7: the improvement of the prediction of the Zener model with nonlinear optimized relaxation times is clearly seen, both in the Fourier amplitude spectra and in the time evolution of the goodness-of-fit scores.

The global (i.e. time- and frequency-averaged) phase and envelope goodness-of-fit scores are given in Table 4 for $N = 3$, 4, 6, 10. They confirm (i) that the phase misfits are negligible after the adjustment of the physical dispersion at the reference frequency and (ii) that for $N \geq 4$ mechanisms, the solution of the Zener model with nonlinear optimization of the relaxation times matches the solution of the constant Q model almost perfectly, whereas $N \geq 6$ mechanisms are needed to obtain the same accuracy when the relaxation times are computed based on classical linear optimization.

5 CONCLUSIONS AND FUTURE WORK

We have developed a nonlinear methodology based on the *SolvOpt* algorithm of Kappel & Kuntsevich (2000) to optimize the coefficients of the Zener viscoelastic model that is significantly more accurate, for a given number of relaxation mechanisms, than the classical linear approach of Emmerich & Korn (1987), or equivalently that can reach similar accuracy for a smaller number of relaxation mechanisms. The approach also ensures the positivity of the coefficients obtained, thus always honouring the constraint of decay of total energy with time and resulting in a stable algorithm when used in viscoelasticity applications, even in the case of very strong attenuation. We have illustrated the improved accuracy obtained based on several numerical experiments, first for a simple wave pulse propagating in a homogeneous 1-D medium with strong attenuation and then for a more realistic 3-D wavefield propagating in a stratified medium with large contrasts in seismic velocities and attenuation.

In future work, we plan to extend our applications of this technique to fitting a non-constant $Q(\omega)$ profile; such an extension could be useful, for example, for non-destructive testing or in ocean acoustics. Since the approach used is not specific to the Zener model, we also plan to apply it to other, more complex or less classical models, which may even involve fractional derivatives (e.g. Zhu & Carcione 2014); in viscoelasticity, one can think of the Andrade model (e.g. Ben Jazia *et al.* 2014), the fractional Kelvin–Voigt model (Caputo 1967) or the fractional Zener model (Nasholm & Holm 2013), and in poroelasticity of the widely used model based on the Biot–Johnson–Koplik–Dashen theory (e.g. Blanc *et al.* 2013).

Our SEISMIC_CPML finite-difference and SPECFEM spectral-element software packages are available open source at geodynamics.org; they both include our implementation of the *SolvOpt* technique presented in this paper.

ACKNOWLEDGEMENTS

The *SolvOpt* algorithm was developed by Franz Kappel and Alexei V. Kuntsevich in Kappel & Kuntsevich (2000). We thank Pierre Suquet for introducing us to the article of Rekik & Brenner (2011),

and Chang-Hua Zhang, Eric Rosenkrantz and Cédric Bellis for fruitful discussion. We thank the two reviewers Jozef Kristek and José M. Carcione for useful comments that improved the manuscript. Calculations were performed using the computing resources of the CIMENT infrastructure. Part of this work was funded by the Simone and Cino del Duca / Institut de France / French Academy of Sciences Foundation under grant #095164, by the European 'Mont-Blanc: European scalable and power efficient HPC platform based on low-power embedded technology' #288777 project of call FP7-ICT-2011-7 and by the European 'WAVES: Waves and Wave-Based Imaging in Virtual and experimental Environments' #641943 project of call H2020-MSCA-ITN-2014. ZX thanks the continuous support of Prof Liao Zhenpeng, the China Scholarship Council for financial support during his stay at LMA CNRS, and the NSF of the Heilongjiang Province of China under grant #LC201403.

REFERENCES

Asvadurov, S., Knizhnerman, L. & Pabon, J., 2004. Finite-difference modeling of viscoelastic materials with quality factors of arbitrary magnitude, *Geophysics,* **69**(3), 817–824.

Bécache, E., Ezziani, A. & Joly, P., 2004. A mixed finite element approach for viscoelastic wave propagation, *Comput. Geosci.,* **8,** 255–299.

Ben Jazia, A., Lombard, B. & Bellis, C., 2014. Wave propagation in a fractional viscoelastic Andrade medium: diffusive approximation and numerical modeling, *Wave Motion,* **51**(6), 994–1010.

Bielak, J., Karaoglu, H. & Taborda, R., 2011. Memory-efficient displacement-based internal friction for wave propagation simulation, *Geophysics,* **76**(6), T131–T145.

Blanc, E., Chiavassa, G. & Lombard, B., 2013. Biot-JKD model: simulation of 1D transient poroelastic waves with fractional derivatives, *J. Comput. Phys.,* **237,** 1–20.

Bouchon, M., 1981. A simple method to calculate Green's functions for elastic layered media, *Bull. seism. Soc. Am.,* **71,** 959–971.

Cao, D. & Yin, X., 2014. Equivalence relations of generalized rheological models for viscoelastic seismic-wave modeling, *Bull. seism. Soc. Am.,* **104**(1), 260–268.

Caputo, M., 1967. Linear models of dissipation whose *Q* is almost frequency independent: Part II, *Geophys. J. R. astr. Soc.,* **13,** 529–539.

Carcione, J.M., 1993. Seismic modeling in viscoelastic media, *Geophysics,* **58**(1), 110–120.

Carcione, J.M., 2001. *Wave Fields in Real Media: Wave Propagation in Anisotropic, Anelastic and Porous Media,* 1st edn, Elsevier Science.

Carcione, J.M., 2014. *Wave Fields in Real Media: Wave Propagation in Anisotropic, Anelastic, Porous and Electromagnetic media,* 3rd edn, Elsevier Science.

Carcione, J.M., Kosloff, D. & Kosloff, R., 1988a. Wave propagation simulation in a linear viscoelastic medium, *Geophys. J. Int.,* **95,** 597–611.

Carcione, J.M., Kosloff, D. & Kosloff, R., 1988b. Viscoacoustic wave propagation simulation in the Earth, *Geophysics,* **53**(6), 769–777.

Carcione, J.M., Cavallini, F., Mainardi, F. & Hanyga, A., 2002. Time-domain modeling of constant-*Q* seismic waves using fractional derivatives, *Pure appl. Geophys.,* **159,** 1719–1736.

Casula, G. & Carcione, J.M., 1992. Generalized mechanical model analogies of linear viscoelastic behaviour, *Bollettino di Geofisica Teorica ed Applicata,* **34**(136), 235–256.

Chaljub, E. *et al.*, 2015. 3-D numerical simulations of earthquake ground motion in sedimentary basins: testing accuracy through stringent models, *Geophys. J. Int.,* **201**(1), 90–111.

Coutant, O., 1989. Program of numerical simulation AXITRA, Tech. rep., LGIT, Université Joseph Fourier, Grenoble, France, (in French).

Dahlen, F.A. & Tromp, J., 1998. *Theoretical Global Seismology,* Princeton Univ. Press.

Day, S.M., 1998. Efficient simulation of constant *Q* using coarse-grained memory variables, *Bull. seism. Soc. Am.,* **88,** 1051–1062.

Day, S.M. & Bradley, C., 2001. Memory-efficient simulation of anelastic wave propagation, *Bull. seism. Soc. Am.,* **91,** 520–531.

Day, S.M. & Minster, J.B., 1984. Numerical simulation of attenuated wavefields using a Padé approximant method, *Geophys. J. R. astr. Soc.,* **78**(1), 105–118.

Dhemaied, A., Rejiba, F., Camerlynck, C., Bodet, L. & Guérin, R., 2011. Seismic-wave propagation modeling in viscoelastic media using the auxiliary differential equation method, *Bull. seism. Soc. Am.,* **101**(1), 413–420.

Emmerich, H. & Korn, M., 1987. Incorporation of attenuation into time-domain computations of seismic wave fields, *Geophysics,* **52,** 1252–1264.

Favrie, N., Lombard, B. & Payan, C., 2015. Fast and slow dynamics in a nonlinear elastic bar excited by longitudinal vibrations, *Wave Motion,* **56,** 221–238.

Graves, R.W. & Day, S.M., 2003. Stability and accuracy of coarse-grain viscoelastic simulations, *Bull. seism. Soc. Am.,* **93,** 283–300.

Groby, J.P. & Tsogka, C., 2006. A time domain method for modeling viscoacoustic wave propagation, *J. Comput. Acoust.,* **14**(2), 201–236.

Kappel, F. & Kuntsevich, A., 2000. An implementation of Shor's *r*-algorithm, *Comput. Optim. Appl.,* **15**(2), 193–205.

Käser, M., Dumbser, M., De La Puente, J. & Igel, H., 2007. An arbitrary high-order discontinuous Galerkin method for elastic waves on unstructured meshes—III. Viscoelastic attenuation, *Geophys. J. Int.,* **168**(1), 224–242.

Kjartansson, E., 1979. Attenuation of seismic waves in rocks and applications in energy exploration, *PhD thesis,* Stanford University, California, USA.

Komatitsch, D. & Tromp, J., 1999. Introduction to the spectral-element method for 3-D seismic wave propagation, *Geophys. J. Int.,* **139**(3), 806–822.

Komatitsch, D., Liu, Q., Tromp, J., Süss, P., Stidham, C. & Shaw, J.H., 2004. Simulations of ground motion in the Los Angeles basin based upon the spectral-element method, *Bull. seism. Soc. Am.,* **94**(1), 187–206.

Kristek, J. & Moczo, P., 2003. Seismic-wave propagation in viscoelastic media with material discontinuities: a 3D fourth-order staggered-grid finite-difference modeling, *Bull. seism. Soc. Am.,* **93**(5), 2273–2280.

Kristeková, M., Kristek, J. & Moczo, P., 2009. Time-frequency misfit and goodness-of-fit criteria for quantitative comparison of time signals, *Geophys. J. Int.,* **178**(2), 813–825.

Liu, P. & Archuleta, R.J., 2006. Efficient modeling of *Q* for 3D numerical simulation of wave propagation, *Bull. seism. Soc. Am.,* **96**(4A), 1352–1358.

Liu, H.P., Anderson, D.L. & Kanamori, H., 1976. Velocity dispersion due to anelasticity: implications for seismology and mantle composition, *Geophys. J. R. astr. Soc.,* **47,** 41–58.

Lombard, B. & Piraux, J., 2011. Numerical modeling of transient two-dimensional viscoelastic waves, *J. Comput. Phys.,* **230**(15), 6099–6114.

Mainardi, F., 2010. *Fractional Calculus and Waves in Linear Viscoelasticity: An Introduction to Mathematical Models,* Imperial College Press.

Martin, R. & Komatitsch, D., 2009. An unsplit convolutional perfectly matched layer technique improved at grazing incidence for the viscoelastic wave equation, *Geophys. J. Int.,* **179**(1), 333–344.

Moczo, P. & Kristek, J., 2005. On the rheological models used for time-domain methods of seismic wave propagation, *Geophys. Res. Lett.,* **32,** L01306, doi:10.1029/2004GL021598.

Nasholm, S.P. & Holm, S., 2013. On a fractional Zener elastic wave equation, *Fract. Calc. Appl. Anal.,* **16,** 26–50.

Petersson, N.A. & Sjögreen, B., 2012. Stable and efficient modeling of anelastic attenuation in seismic wave propagation, *Commun. Computat. Phys.,* **12,** 193–225.

Peyrusse, F., Glinsky, N., Gélis, C. & Lanteri, S., 2014. A nodal discontinuous Galerkin method for site effects assessment in viscoelastic media: verification and validation in the Nice basin, *Geophys. J. Int.,* **199,** 315–334.

Rekik, A. & Brenner, R., 2011. Optimization of the collocation inversion method for the linear viscoelastic homogenization, *Mech. Res. Commun.,* **38**(4), 305–308.

Robertsson, J.O.A., 1996. A numerical free-surface condition for elastic/viscoelastic finite-difference modeling in the presence of topography, *Geophysics,* **61**(6), 1921–1934.

Robertsson, J.O.A., Blanch, J.O. & Symes, W.W., 1994. Viscoelastic finite-difference modeling, *Geophysics,* **59**(9), 1444–1456.

Russo, G. & Zollo, A., 2003. A constant-Q technique for the numerical simulation of attenuation of seismic body waves, *Geophysics,* **68**(5), 1744–1748.

Savage, B., Komatitsch, D. & Tromp, J., 2010. Effects of 3D attenuation on seismic wave amplitude and phase measurements, *Bull. seism. Soc. Am.,* **100**(3), 1241–1251.

Shor, N., 1985. *Minimization Methods for Non-Differentiable Functions,* Springer-Verlag.

van Driel, M. & Nissen-Meyer, T., 2014. Optimized viscoelastic wave propagation for weakly dissipative media, *Geophys. J. Int.,* **199**(2), 1078–1093.

Withers, K.B., Olsen, K.B. & Day, S.M., 2015. Memory-efficient simulation of frequency-dependent Q, *Bull. seism. Soc. Am.,* **105**(6), 3129–3142.

Xu, T. & McMechan, G.A., 1998. Efficient 3-D viscoelastic modeling with application to near-surface land seismic data, *Geophysics,* **63**(2), 601–612.

Zhu, T. & Carcione, J.M., 2014. Theory and modelling of constant-Q P- and S-waves using fractional spatial derivatives, *Geophys. J. Int.,* **196**(3), 1787–1795.